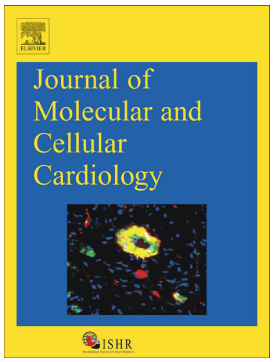
Journal Pre-proof



Functional recruitment and regulatory mechanisms of SK channels in patients with early stages of ventricular remodeling

Alba Pérez-Martínez, Cristina López-Andrés, Laura García-Mendívil, Marta López-Yus, Diana Batín, Jose M. Vallejo-Gil, Javier Fañanás-Mastral, Manuel Vázquez-Sancho, Marta Matamala-Adell, Juan F. Sorribas-Berjon, Javier A. Bellido-Morales, Carlos Ballester-Cuenca, Jose M. Arbonés Mainar, Esther Pueyo, Aída Oliván-Viguera

PII: S0022-2828(26)00099-4

DOI: https://doi.org/10.1016/j.yjmcc.2026.07.002

Reference: YJMCC 10052

To appear in: *Journal of Molecular and Cellular Cardiology*

Received date: 14 December 2025

Revised date: 10 May 2026

Accepted date: 6 July 2026

Please cite this article as: A. Pérez-Martínez, C. López-Andrés, L. García-Mendívil, et al., Functional recruitment and regulatory mechanisms of SK channels in patients with early stages of ventricular remodeling, *Journal of Molecular and Cellular Cardiology* (2026), https://doi.org/10.1016/j.yjmcc.2026.07.002

This is a PDF of an article that has undergone enhancements after acceptance, such as the addition of a cover page and metadata, and formatting for readability. This version will undergo additional copyediting, typesetting and review before it is published in its final form. As such, this version is no longer the Accepted Manuscript, but it is not yet the definitive Version of Record; we are providing this early version to give early visibility of the article. Please note that Elsevier's sharing policy for the Published Journal Article applies to this version, see: https://www.elsevier.com/about/policies-and-standards/sharing#4-published-journal-article. Please also note that, during the production process, errors may be discovered which could affect the content, and all legal disclaimers that apply to the journal pertain.

© 2026 Published by Elsevier Ltd.

Journal Pre-proof

Title

Functional recruitment and regulatory mechanisms of SK channels in patients with early stages of ventricular remodeling

Authors

Alba Pérez-Martínez* [a,b,c], Cristina López-Andrés [a,c], Laura García-Mendívil [a,c], Marta López-Yus [c,d,e,f], Diana Batín [g], Jose M. Vallejo-Gil [g], Javier Fañanás-Mastral [g], Manuel Vázquez-Sancho [g], Marta Matamala-Adell [g], Juan F. Sorribas-Berjon [g], Javier A. Bellido-Morales [g], Carlos Ballester-Cuenca [g], Jose M. Arbonés Mainar [c,d,e,f], Esther Pueyo [a,b,c], Aída Oliván-Viguera* [a,b,c].

[a] Biomedical Signal Interpretation and Computational Simulation Group (BSICoS), Aragón Institute of Engineering Research (I3A). Edificio I+D+I C/Mariano Esquillor s/n, 50018 Zaragoza, Spain

[b] Biomedical Research Networking Center in Bioengineering, Biomaterials and Nanomedicine (CIBER-BBN), 50018 Zaragoza, Spain

[c] Instituto de Investigación Sanitaria (IIS) Aragón, 50009 Zaragoza, Spain

[d] Adipocyte and Fat Biology Laboratory (AdipoFat), Translational Research Unit, University Hospital Miguel Servet, 50009 Zaragoza, Spain

[e] Aragón Institute of Health Sciences (IACS), 50009, Zaragoza, Spain

[f] CIBER Physiopathology of Obesity and Nutrition (CIBERObn), Instituto Salud Carlos III, 28029 Madrid, Spain

[g] Department of Cardiovascular Surgery, University Hospital Miguel Servet, Zaragoza 50009, Spain

*Corresponding authors

***Alba Pérez-Martínez**: perezma@unizar.es

Cristina López-Andrés: cristina.lopez@unizar.es

Laura García-Mendívil: lgmendivil@unizar.es

Marta López-Yus: martalyus@gmail.com

Diana Batín: dcbatin@salud.aragon.es

Jose M. Vallejo-Gil: jvallejo@salud.aragon.es

Javier Fañanás-Mastral: jfananas@salud.aragon.es

Manuel Vázquez-Sancho: drmvazquez@yahoo.es

Marta Matamala-Adell: mmatamala80@hotmail.com

Journal Pre-proof

Journal Pre-proof

Juan F. Sorribas-Berjon: juanfernandosorribas@gmail.com

Javier A. Bellido-Morales: jabellido@salud.aragon.es

Carlos Ballester-Cuenca: cballester@salud.aragon.es

Jose M. Arbonés Mainar: jmarbones.iacs@aragon.es

Esther Pueyo: epueyo@unizar.es

***Aída Oliván-Viguera**: aidaolivanviguera@gmail.com

Journal Pre-proof

Journal Pre-proof

Abstract

Aims:

Small-conductance Ca^{2+}-activated potassium channels (SK) are increasingly investigated as therapeutic targets for atrial fibrillation. Emerging evidence, however, indicates their functional relevance in ventricular pathologies. This study investigates the expression, localization, and functional role of SK2 and SK3 channel subtypes in ventricular myocardium from patients with and without valvular disease-associated remodeling.

Methods and results:

Human ventricular tissue was obtained from 125 patients undergoing cardiac surgery. mRNA levels of *KCNN2* and *KCNN3* were quantified with RT-qPCR. Protein levels and localization of SK2 and SK3 were analyzed via immunohistochemistry. Functional responses were evaluated by optical mapping of living ventricular myocardial slices.

Gene expression was not significantly altered in remodeled myocardium. SK2 and SK3 were located in striated patterns, colocalizing with L-type Ca^{2+} channels in all patients. SK3 was also present at intercalated discs, although this pattern was significantly reduced in remodeled myocardium. Functionally, SK channels were inactive in non-remodeled myocardium, with neither apamin nor SKA-31 altering action potential duration (APD). In contrast, in remodeled myocardium, apamin prolonged and SKA-31 shortened APD. This response to SKA-31 was more pronounced in patients with reduced ejection fraction. Mechanistically, SKA-31 effects were abolished by L-type Ca^{2+} channel blockade or CaMKII inhibition, but not by PKA inhibition, suggesting that SK activation is Ca^{2+} and CaMKII-dependent.

Conclusions:

SK channels become functionally upregulated in the early stages of ventricular remodeling despite the absence of gene expression changes. SK activation might rely on post-translational modifications and calcium handling alterations. These findings highlight the need for caution in targeting SK channels therapeutically.

Keywords

Optical mapping

Cardiac slices

SK channels

Ventricular remodeling

Repolarization

1. Introduction

Small-conductance Ca^{2+}-activated potassium (SK) channels, encoded by the *KCNN* gene family, comprise three isoforms (SK1-3). These channels are voltage-independent and are gated exclusively by intracellular Ca^{2+} through constitutive binding to calmodulin (CaM). Upon Ca^{2+} binding, CaM undergoes a conformational change that opens the channel pore, allowing K^+ efflux and contributing to membrane repolarization. SK channels thus form a direct mechanistic link between intracellular Ca^{2+} dynamics and the cardiac action potential (AP) [1,2].

SK channels are selectively blocked by apamin, which has been traditionally used for the study of these channels [3]. Of the three isoforms, SK2 and SK3 are expressed in the human heart, predominantly in atrial tissue [1,4]. SK channel inhibition prolongs AP duration (APD) in atrial cardiomyocytes while having minimal effects in ventricular cardiomyocytes [5]. Based on this atria selectivity, SK channels have been proposed as promising targets for atrial-specific antiarrhythmic therapy [6–8]. A phase II clinical trial of the SK channel inhibitor AP30663 demonstrated encouraging results in terminating recent-onset atrial fibrillation (AF) episodes [9].

Nonetheless, increasing evidence suggests that SK channels are also expressed and functionally relevant in the ventricular myocardium, particularly under pathological conditions such as hypertrophy and heart failure [10–16]. While SK channels are not thought to contribute significantly to ventricular repolarization in the healthy ventricle, their upregulation in disease states may modulate ventricular electrophysiology. Whether this is proarrhythmic or antiarrhythmic remains unclear [11,17]. Some studies suggest a protective SK role in preserving repolarization reserve, while others implicate SK channels in promoting repolarization heterogeneity and arrhythmogenesis.

SK channels are subject to complex regulation at transcriptional and post-translational levels, affecting their trafficking, membrane localization, and Ca^{2+} sensitivity. They assemble as tetramers and can form heteromers, notably between SK2 and SK3 subunits [4]. SK channels are part of supramolecular complexes. CaM‘s Ca^{2+} sensitivity is modulated via phosphorylation by casein kinase 2 (CK2) and dephosphorylation by protein phosphatase 2A (PP2A). SK channels also associate with L-type calcium channels (LTCCs) through α-actinin2 and are spatially organized near ryanodine receptors (RyRs) in the junctional sarcoplasmic reticulum [7, 18–21]. Ca^{2+}/CaM-dependent protein kinase II (CaMKII) enhances SK channel Ca^{2+} sensitivity via phosphorylation, especially under pathological conditions with altered Ca^{2+} handling [22–24]. In contrast, phosphorylation by protein kinase A (PKA) reduces SK channel membrane expression and mitigates voltage-dependent deactivation at high Ca^{2+} concentrations [25]. These signaling pathways work in concert to finely tune SK channel activity in response to acute and chronic alterations in intracellular Ca^{2+} and cyclic adenosine monophosphate levels.

To date, most studies on ventricular SK channels in humans have been limited to patients with end-stage heart failure undergoing heart transplantation or left ventricular assist device implantation. These models often reflect advanced disease states and offer limited insight into earlier stages of ventricular remodeling. Additionally, most studies use isolated cardiomyocytes, which may disrupt native subcellular architecture and cell-cell interactions critical for proper SK channel localization and function. Our group recently developed a minimally invasive approach to assess ventricular electrophysiology in living human tissue using thin cardiac slices obtained from small biopsies [26]. This method allows for the concurrent evaluation of gene and protein expression, subcellular localization, and electrophysiological properties in tissues from patients with varying degrees of cardiac remodeling.

In this study, we characterized the expression, distribution, and function of SK2 and SK3 channels in ventricular myocardium from patients with and without valvular disease-associated remodeling. *KCNN2* and *KCNN3* mRNA levels did not differ significantly between groups. Immunohistochemistry revealed consistent expression of SK2 and SK3 in all samples, with SK2 and SK3 displaying a striated distribution pattern indicative of T-tubule localization. In some samples, SK3 was additionally localized to intercalated discs. Optical mapping demonstrated that SK channel activation and inhibition occurred only in remodeled tissue. Furthermore, we identified key roles for CaMKII and PKA signaling in modulating SK channel activity in the context of ventricular remodeling.

2. Methods

2.1 Human ventricular tissue extraction and processing

125 human transmural core biopsies and papillary muscles were obtained by experienced cardiothoracic surgeons at Miguel Servet University Hospital, Zaragoza, Spain. Biopsies were collected during valve replacement or coronary artery bypass grafting surgeries after cardioplegic arrest with Celsior, as previously described [26]. All patients gave written informed consent before surgery and prior to their inclusion in the study. The study conforms to the principles outlined in the Declaration of Helsinki and was approved by the local Ethics Committee (CEICA, reference number PI17/0023).

Upon collection, papillary muscles and transmural biopsies were rapidly submerged in cold Tyrode's solution (composition in mM: NaCl 140, KCl 6, CaCl2 1.8, MgCl2 (·6H2O) 1, glucose 10, HEPES 10) supplemented with 30 mM 2, 3-butanedione monoxime (BDM), pH adjusted to 7.4, all chemicals from Sigma Aldrich (Mo, USA). Samples were transported to the laboratory within 30 minutes.

Transmural biopsies were taken from the epicardial surface of the left ventricular wall or the transmural septum and their length varied between 0.5 and 1 cm. The alignment of the fibers was

identified, and biopsies were embedded in 4% low-melting agarose (Ecogen, Spain), ensuring that the fiber alignment was parallel to the slicing plane, and glued (LOCTITE, Henkel Iberica, Spain) to the vibratome cutting stage. In the transmural biopsies obtained from the epicardial surface of the ventricular wall, only the first millimeter from the epicardial surface was considered as epicardial tissue. Papillary muscles were directly glued onto the vibratome cutting stage with the chordae tendinae aligned with the slicing plane or, when necessary to assure the correct longitudinal alignment of muscle fibers, embedded in 4% low-melting agarose.

350-µm-thick slices were produced with a high precision vibratome (Leica VT1200S, Leica Microsystems, Germany) with stainless steel blade (Astra Superior Platinum double edge razor blades, Gillette, USA) advancing at a speed of 0.03-0.04 mm/s and oscillating at an amplitude of 2 mm and a vibrating frequency of 80 Hz, submerged in cold Tyrode's supplemented with 30 mM BDM. Thicker sections (0.5-2 mm) were cut and immediately snap frozen for gene expression evaluation or fixed and embedded in paraffin for histological analysis. To enable evaluation of equivalent transmural layers between remodeled and non-remodeled patients, stored samples were also used for histological evaluation.

2.2 Quantitative real-time PCR

A total number of 43 heart tissue samples were snap frozen in liquid nitrogen and stored at -80 ºC until RNA extraction. The clinical characteristics of patients can be consulted in Table S1. Samples were placed in pre-cooled tubes containing TRIzol reagent (Sigma, USA) and rapidly subjected to manual homogenization using a pestle. Total RNA extraction was carried out using standard procedure according to the manufacturer's instructions (QIAGEN, Denmark). All the RNA samples were then treated with RNase-Free DNase (Life Technologies, USA) to remove genomic DNA. RNA was reverse-transcribed using PrimeScript Reverse Transcriptase (Takara Bio, Japan). Real-time PCR was performed using the StepOnePlus system (Applied Biosystems, USA). 2 µl of the cDNA product was amplified using gene-specific primers in a total volume of 15 µl per reaction with SYBR Select Master Mix (Applied Biosystems, USA), using a protocol as follows: 95°C for 10 min, 40 cycles of 15 sec at 95°C and 1 min at 60°C, and 15 sec at 95°C. mRNA expression of *GAPDH*, *CACNA1C*, *KCND3*, *KCNJ2*, *KCNH2*, *KCNQ1*, *KCNN2* and *KCNN3* were analyzed, primer sequence can be consulted in Table S2, *KCNN2* primers were kindly provided by Natalia Hernandez Bellido and Laura Ordovás. Relative gene expression was normalized to *GAPDH* expression using the $2^{-\triangle\triangle Ct}$ method.

2.3 Immunohistochemistry

Tissue sections from 83 patients were fixed in 4% paraformaldehyde for 1 hour at 4ºC and subsequently stored in PBS with 0.01% Na-Azide at 4ºC until paraffin embedding. 3-µm-thick sections were stained following standard immunohistochemical procedures. The clinical

characteristics of patients can be consulted in Table S3. Briefly, sections were deparaffinated and rehydrated. Antigen retrieval was performed with TRIS/EDTA buffer (pH = 9) with 0.05% TWEEN-20 at 97ºC for 20 minutes. After cooling sections were blocked with PBS containing 5% bovine serum albumin (BSA) for 1 hour. Primary antibodies were incubated overnight at 4ºC and secondary antibodies together with wheat germ agglutinin (WGA) were incubated at room temperature (RT) for 1 hour. Two treatments were performed to reduce autofluorescence: glycine 1M for 30 minutes at RT and a final staining with Sudan Black 1% in 70% ethanol for 20 minutes. Samples were mounted with Fluoromount G (Invitrogen, USA).

Primary antibodies were goat polyclonal anti-KCNN2 (SK2, dilution 1:125) (PA5-19205, Invitrogen, USA), rabbit polyclonal anti-KCNN3 (SK3, dilution 1:125) (PA5-41014, Invitrogen, USA) and mouse monoclonal recombinant anti-Cav1.2 Ca2+ channel (L-Type Ca^{2+} channels, dilution 1:125) (184183-rAb, Addgene, USA). Secondary antibodies were Alexa Fluor 488 donkey anti-goat IgG (dilution 1:200) (A11055, Molecular Probes, USA), CFTM-633 donkey anti-rabbit (dilution 1:200) (SAB4600132, Sigma-Aldrich, USA) and Alexa Fluor 568 donkey anti-mouse IgG (dilution 1:200) (A10037, Thermofischer, Spain). Extracellular matrix was stained with WGA conjugated with Alexa-fluor 488 or 633 (dilution 1:1000) (W32464, Thermofischer, Spain and 29024-1, Biotium, USA, respectively).

Tissue sections were imaged using confocal microscopy Carl Zeiss LSM 880 (Carl Zeiss, Germany). Z-series of images were collected for the whole thickness of the slice. Using ImageJ, 2-3 line scans were extracted per image for each channel (SK2/ L-Type Ca^{2+} channels and SK3/ L-Type Ca^{2+} channels). A custom MATLAB script was developed to identify the maximum intensity peaks in the L-type channel, which correspond with the location of striations. For each peak, the maximum intensity of SK2 or SK3 was measured within a 3-pixel window (0.63 µm). Subsequently, the intensity values from all peaks across all line scans were averaged for each patient to obtain a representative value (15 to 40 peaks were averaged from each patient). In the case of L-Type Ca^{2+} channels and SK3 co-staining, an additional qualitative scoring of SK3 location at intercalated discs was performed by two independent observers. Each observer gave a scoring of 0 (not present), 1 (limited) or 2 (clearly present) for the expression of SK3 in the intercalated discs. The inter observer agreement was tested with Cohen's kappa coefficient test, and the scorings of the two observers were summed for further evaluation. For each staining, only samples with a striated pattern in the L-Type Ca^{2+} channels were considered for evaluation.

2.4 Optical mapping of transmembrane potential and data analysis

For the optical mapping recordings, 350-µm-thick slices were incubated in Tyrode's solution at RT with the excitation-contraction uncoupler 10 µM blebbistatin (Tocris Bioscience, USA) for 30 minutes and with the voltage-sensitive dye 7.5 µM RH237 (Invitrogen, USA) for 15 minutes.

Slices were washed in Tyrodes's solution at RT for at least 30 minutes before the recording of transmembrane potential, the functional evaluation was performed within 1 to 8 hours of the slice production.

Myocardial tissue slices from 79 patients (Table S4) were optically mapped with a MiCAM O5-Ultima CMOS camera (SciMedia, USA) with a spatial resolution of 100 x 100 pixels with 3.1 μm per pixel and a temporal resolution of 2 ms. Measurements were conducted in a heated chamber (RC-27NE in a PM-6 heated platform, Warner Instruments, USA) at 37˚ C equipped with two platinum field-stimulation electrodes in Tyrode's solution. 20-second recordings were acquired at 0.5, 1, and 2 Hz at baseline conditions and after the addition of the different compounds (100 nM isoprenaline, 1 μM apamin, 100 μM SKA-31, 10 μM nifedipine, 2 μM KN-93, 10 μM AIP, and 2 μM H-89), slices were allowed to stabilize for 3 minutes at a pacing frequency of 0.5 Hz before each set of recordings.

The evaluation of the optical mapping signals was performed with OMap, a custom-write software based on MATLAB [27]. Briefly, this software filtered the optically mapped signals to remove the baseline drift by high pass filtering as well as noise and artifacts with spatio-temporal Gaussian filtering. For each pixel, the signal-to-noise ratio (SNR) was computed as the ratio between the peak AP amplitude and the root-mean-square of the diastolic signal, and only the pixels exceeding a predefined SNR threshold were included in the analysis. In addition, a morphology-based criteria was included to ensure the physiological consistency of the signals. Specifically, for each pixel, APs were temporally aligned and averaged, and their morphology was evaluated ensuring adequate return to baseline. Upstroke and downstroke characteristics were also evaluated. Upstroke quality was assessed based on the consistency and timing of the maximum first derivative, ensuring a well-defined depolarization phase, while downstroke morphology was evaluated by analyzing the repolarization segment to confirm a stable return to baseline. Only pixels fulfilling all these criteria were included in the final maps. A map with the values of APD at 80% repolarization (APD_{80}) for all included pixels was obtained.

2.5 Statistical analysis

Statistical comparisons were performed using nonparametric tests, as the limited sample size and the distribution of the data did not generally satisfy the assumptions of normality when tested with the Shapiro-Wilk test. Comparison of the continuous variables between two groups was performed using Mann-Whitney test for unpaired samples or Wilcoxon signed-rank test for paired samples both tests were two sided. A p value < 0.05 was considered for statistically significance. Significant differences were represented as * ($p < 0.05$), ** ($p < 0.01$), *** ($p < 0.001$) or **** ($p < 0.0001$). Graphs were produced with GraphPad Prism 8 Software unless stated otherwise.

For the optical mapping evaluation, the notation n/N was used to denote n tissue slices from N patients. From transmembrane voltage recordings, APD was calculated at 80% repolarization (APD_{80}). In the APD graphics, each point represents the average value of APD_{80}, or normalized APD_{80}, for each patient and treatment. 2 to 5 slices were evaluated per patient and condition. In the text, data from all patients are presented as median [25^{th} and 75^{th} percentiles].

3. Results

Control samples (non-remodeled myocardium) were collected from ischemia-free regions in patients undergoing coronary artery bypass grafting who exhibited preserved left ventricular ejection fraction (LVEF, > 50 %), no valvular dysfunction, no ventricular hypertrophy (ventricular mass index < 160 g/m^2 or clinical diagnosis), and no clinical signs of dilated cardiomyopathy. Remodeled samples were collected from patients undergoing surgery for clinically diagnosed valvular heart disease (aortic and/or mitral stenosis or insufficiency). This group included patients with preserved or reduced LVEF, as well as with or without ventricular hypertrophy.

3.1 Gene expression

mRNA expression levels of genes from the main channels involved in cardiac AP (*CACNA1C, KCND3*, *KCNJ2*, *KCNH2*, *KCNQ1*) as well as *KCNN2* and *KCNN3* genes were determined by real-time PCR. Midmyocardial tissue samples of 9 patients without ventricular remodeling and 24 papillary muscles and 10 septal samples from patients with ventricular remodeling were studied. The clinical characteristics of patients can be consulted in Table S1. All samples showed mRNA levels within range of cycle threshold (Ct) values of 18 and 30. Only *CACNA1C* showed significantly different expression levels between transmural biopsies from patients without ventricular remodeling and papillary muscles from patients with ventricular remodeling (Figure 1A). No differences were found in *CACNA1C* expression levels between non-remodeled myocardium and remodeled interventricular septum. Expression levels of *KCND3*, *KCNJ2*, *KCNH2*, *KCNQ1*, *KCNN2* and *KCNN3* levels did not significantly vary between non-remodeled myocardium (mid-myocardium) and remodeled myocardium (septal biopsies and papillary muscles) (Figure 1B to 1G).

3.2 Protein expression

Co-staining of LTCCs and SK2 or SK3 were performed in a subset of 73 patients. The clinical characteristics of patients can be consulted in Table S2. Both SK2 (Figure 2A) and SK3 (Figure 3A) proteins were detected in a striated pattern in cardiomyocytes, consistent with localization along the T-tubules, and showed colocalization with LTCCs. No evidence of non-specific signal was detected in the SK2 or SK3 channels in negative control samples containing only secondary antibodies (Figures S1 and S2). SK2 expression in the non-remodeled epicardium was

significantly higher than in the remodeled epicardium and papillary muscles (Figure 2B). No statistically significant differences in SK2 fluorescence intensity were observed among the different regions of remodeled myocardium (epicardium, papillary muscles, and interventricular septum). Within remodeled patients, only significant differences in expression levels were found in patients with mitral valvulopathy (8070 [6396, 9831], N = 31), which presented reduced protein expression with respect to patients without mitral valvulopathy (9841 [8826, 12118], N = 39). Remodeled patients with additional right side valvular dysfunction also presented significantly ($p = 0.0194$) lower levels of SK2 protein expression (7808 [6345, 8603], N = 10) than patients without right side valvular dysfunction (9415 [8107, 11617], N = 60). In addition to its striated distribution, SK2 channels were also detected in the intercalated disks in a small number of patients (Figure 2C). The inter-observer agreement for the scoring of SK2 location in the intercalated discs was 0.746 and there were no statistically significant differences between the different groups.

SK3 expression in striations was higher in the remodeled epicardium than in non-remodeled epicardium. However, the difference did not reach statistical significance. In contrast, SK3 protein expression levels in the striations were significantly higher in the remodeled epicardium than in the papillary muscles and interventricular septum (Figure 3B). Within each remodeled group, we further studied whether the expression levels of SK3 could be explained by factors such as: sex, left ventricular ejection fraction (LVEF), hypertrophy, aortic valvulopathy, mitral valvulopathy, right side valvular disfunction (RSVD), high blood pressure (HBP), dyslipidemia (DLD), treatment with β-blockers, treatment with angiotensin converting enzyme or angiotensin receptor blockers (ACEI or ARBs), diabetes (DBT) or age. Within each group, none of these factors influenced the expression levels of SK3.

In addition to its striated distribution, SK3 channels were also detected in the intercalated disks in more patients than SK2. The inter-observer agreement for the scoring of SK3 location in the intercalated discs was 0.723. SK3 channel presence in the intercalated discs was significantly higher in non-remodeled myocardium than in remodeled epicardium ($p = 0.0099$), remodeled papillary muscles ($p = 0.0008$) and remodeled septum ($p = 0.0108$) (Figure 3C). Interestingly, patients with diabetes within the non-remodeled group presented a significantly ($p = 0.0048$) lower score of SK3 present in the intercalated discs (median 3 [1, 4], N = 7 vs 4 [4, 4], N = 9).

3.3 Functional expression

Transmembrane potential was recorded and APD_{80} was measured at different pacing frequencies at baseline conditions and after the addition of several known modulators of SK channels to determine their contribution to ventricular repolarization in 83 patients with and without valvular

disease-associated remodeling. The clinical characteristics of patients can be consulted in Table S3.

3.3.1 Inhibition of SK channels

Transmembrane potential was recorded and APD_{80} was measured at a pacing frequency of 1 Hz, in the presence of 100 nM isoprenaline (iso) and after the addition of 1 μM of the selective SK channel blocker apamin, in 17 patients with and without ventricular remodeling. Recordings were performed in the presence of 100 nM isoprenaline to promote the activation of SK currents and enable the assessment of their contribution to ventricular repolarization. In non-remodeled myocardium, apamin, did not significantly alter APD_{80} (+1.0% [-2.6, +8.1], p = 0.4375). In contrast, in remodeled myocardium apamin produced a significant prolongation of APD_{80} (+5.7% [+2.6, + 11.4], p = 0.0093) (Figure 4).

3.3.2 Activation of SK channels

APD_{80} was measured in baseline conditions and after the addition of 100 μm of the SK channel activator SKA-31 in tissue samples from 41 patients with and without ventricular remodeling stimulated at different pacing frequencies (Figure 5).

SKA-31 100 μM did not significantly alter APD_{80} in non-remodeled myocardium at any pacing frequency (Figure 5A). In remodeled myocardium, however, SKA-31 significantly shortened APD_{80} in both biopsies from the papillary muscles (Figure 5B) and interventricular septum (Figure 5C) at all frequencies tested. The response to SKA-31 measured at 1 Hz pacing was statistically different in non-remodeled myocardium that in remodeled myocardium (p = 0.0045 when compared to the response of all remodeled samples). (Figure 5E). Figure S3 shows representative APD_{80} maps obtained from tru-cut biopsies in remodeled and non-remodeled myocardium at baseline conditions and after the addition of 100 μM SKA-31. This differential response between non-remodeled and remodeled tissues was maintained at 0.5 and 2 Hz (Figures 5D to 5F and Table S5). Interestingly, at a pacing frequency of 1 Hz, the response to SKA-31 was similar between the papillary muscles and the interventricular septum (-12.6% [-17.5, -10.3] vs -12.3% [-16.5, -7.7], p = 0.5474) despite the differences in baseline APD_{80} (254 ms [239, 298] vs. 335 ms [268, 363], p = 0.0302). For this reason, no distinction between types of remodeled tissues was made in the subsequent optical mapping analysis.

Next, the influence of clinical characteristics on the magnitude of the response to SK activation with SKA-31 was investigated. No significant differences in the response to SKA-31 depending on gender, cardiac hypertrophy, presence of left valvular pathology, aortic valvulopathy, mitral valvulopathy, arterial hypertension, dyslipidemia, β-blockers intake, ACEI or ARBs intake or diabetes. The only factor influencing the response to SKA-31 was LVEF. Patients with reduced LVEF (< 50) had significantly (p = 0.0244) greater response to SKA-31 (-19.5% [-19.6, -13.7], n

= 5) than patients with preserved LVEF (-12.1 [-7.4, -16.3], n = 30) (Figures 6A to 6K). Age had a weak correlation with the response, with elder patients showing a reduced response to SKA-31 with respect to younger patients (Figure 6L). Baseline APD_{80} did not show correlation with the response to SKA-31 (Figure 6M).

3.3.3 Regulation of SK channels in remodeled tissue

Due to the differences observed at the functional level between remodeled and non-remodeled tissue, which were not explained by differences in mRNA or protein expression, the mechanisms that could be implicated in this differential functional regulation of SK channels were further investigated. Specifically, in papillary muscles and septum of patients with ventricular remodeling, the effect of 100 µM SKA-31 was analyzed after the addition of several inhibitors of proteins known to regulate the activity of SK channels (Figure 7 and Table S6).

First, we evaluated whether blocking Ca^{2+} entry through LTCCs with 10 µM nifedipine was sufficient to avoid the subsequent activation with SKA-31. In cardiac slices from 10 patients with ventricular remodeling, we observed that nifedipine significantly shortened APD_{80} by -22.0% [-33.67, -12.4], -21.1% [-30.8, -11.5] and -20.0% [-27.0, -12.1] at 0.5, 1 and 2 Hz pacing frequencies, respectively. The subsequent addition of SKA-31 did not significantly alter APD_{80} at 0.5 and 1 Hz and slightly prolonged APD_{80} at 2 Hz pacing frequency (Figure 7A).

We next evaluated other post-transcriptional regulations known to affect SK channel activity. We studied the effect of blocking the activity of CaMKII with 2 µM KN-93 and with 10 µM autocamtide-2-related inhibitory peptide (AIP) as well as the effect of blocking PKA with 2 µM H-89 by incubating the slices for 30 minutes with each compound, respectively. Blocking the activity of CaMKII with 2 µM KN-93 or 10 µM AIP prevented the subsequent activation of SK channels with SKA-31 (Figure 7B and C, respectively). Blocking the activity of PKA with 2 µM H-89 did not prevent the activation with SKA-31 at all frequencies (Figure 7D). The response to SKA-31 was slightly reduced ($p = 0.0204$) when comparing the response to SKA-31 at 1 Hz pacing frequency between slices incubated with H-89 (-7.0% [-12.0, -6.3], n/N = 27/10, Figure 7D) with those without in all patients tested (-12.3% [-16.8, -8.7], n/N = 120/35, Figure 5E). However, in a subset of 5 patients (n/N = 11-13/5), SKA 31 was added in slices with and without prior incubation with H-89 and no significant difference was found ($p > 0.9999$) in the activation of SK channels at 1 Hz pacing frequency (Figure 7E).

4.Discussion

4.1 Experimental approach and patient tissue selection

We assessed the expression, localization, and functional role of ventricular SK channels in myocardial biopsies obtained from living patients, both with and without evidence of ventricular remodeling. The classification of samples with and without ventricular remodeling was based

exclusively on clinical criteria rather than on tissue-level characterization including alterations in gene expression, fibrosis, or cardiomyocyte hypertrophy, which allows a more direct clinical translation of our findings.

In contrast to most studies utilizing animal models or end-stage heart failure tissues (e.g., explanted hearts), our approach enables the investigation of intermediate disease stages in human hearts. Despite their small size, both small biopsies and ultrathin living myocardial slices show good viability and frequently support multiple levels of analysis, including transcriptomic, immunohistochemical, and electrophysiological studies, thereby offering a physiologically relevant view of early or moderate ventricular remodeling [26,28].

4.2 Gene expression of SK and major cardiac ion channels

We quantified the mRNA levels of *KCNN2* (SK2) and *KCNN3* (SK3), along with genes encoding key cardiac ion channels involved in the cardiac AP: *CACNA1C* ($I_{Ca,L}$), *KCND3* (I_{to}), *KCNJ2* (I_{K1}), *KCNH2* (I_{Kr}), and *KCNQ1* (I_{Ks}) (Figure 1). No significant differences were observed in the expression of channel genes between groups, except for *CACNA1C*, which was significantly upregulated in the papillary muscles of patients with ventricular remodeling compared to non-remodeled ventricular tissue. Interestingly, the levels of *CACNA1C*, which encodes the α1C subunit of the LTCCs, were similar between remodeled septal tissue and non-remodeled midmyocardium.

This differential expression pattern for *CACNA1C* contrasts with the stability observed in potassium channel gene expression. While some studies report downregulation of potassium currents, especially I_{to} (*KCND3*) and I_{K1} (*KCNJ2*), in heart failure models [29], others show no significant changes [30]. Our findings suggest that such downregulation may not be present at early stages of remodeling.

Similarly, *KCNN2* and *KCNN3* expression levels remain unchanged in remodeled tissue (Figure 1F and 1G, respectively). This observation contrasts with previous reports of SK channel upregulation in advanced heart failure [10,24,30,31], possibly as a compensatory mechanism for reduced repolarizing currents. However, SK channel expression in non-cardiomyocyte populations (e.g., endothelium, fibroblasts) present in the tissue homogenates may obscure cardiomyocyte-specific alterations. Indeed, some SK channel alterations in endothelium have been described in pathological conditions, where they drive the endothelium-derived hyperpolarizing factor response, contributing to reduced dilatory responses [33,34]. Moreover, transcript levels may not correlate with protein function due to post-transcriptional regulation and channel localization. Thus, further analyses were conducted at the protein and functional levels.

4.3 Immunolocalization of SK2 and SK3 channels in human ventricles

The spatial distribution of SK2 and SK3 channels in human ventricular myocardium remains poorly characterized. Previous studies using isolated cardiomyocytes have reported striated localization of SK2 and SK3 under physiological conditions, consistent with T-tubular location and colocalization with LTCCs and RyRs [19,20,35–37]. Our immunohistochemical analysis confirmed the presence of SK2 and SK3 across all patient samples, with a striated pattern indicative of T-tubular location and colocalization with LTCCs (Figures 2 and 3). Importantly, no T-tubule disorganization was observed in our samples, likely reflecting the early disease stage of our patient cohort.

SK2 protein levels were here found to be slightly but significantly higher in non-remodeled epicardial tissues than in remodeled epicardial tissues (Figure 2B), diverging from previous human and animal studies reporting SK2 upregulation in heart failure or AF [35]. Within remodeled tissues, SK2 channel expression was similar across all regions, and was not affected by sex, age, and other evaluated clinical factors. In contrast, SK3 expression displayed greater regional and remodeling-dependent variability (Figure 3B). Within remodeled hearts, SK3 fluorescence intensity was higher in the epicardium, with lower levels in the papillary muscles and interventricular septum. A trend toward higher SK3 expression was observed in remodeled versus non-remodeled epicardial tissue, although with notable inter-patient variability. While immunohistochemistry is a semi-quantitative technique, it enabled us to detect remodeling-associated differences in SK expression channels.

A novel and significant finding was the frequent localization of SK3 at intercalated discs, a pattern not previously described. While SK2 was found at intercalated discs [3,35] in only a minority of patients (Figure 2C), SK3 presence was substantially more frequent (Figure 3C). Although co-staining with other proteins located in the intercalated disks was not performed, the characteristic pattern and distributions clearly supported this localization. Moreover, no evidence of autofluorescence signal was observed in our negative controls (Figures S1 and S2), further confirming the specificity of the staining. In remodeled myocardium, SK3 expression at intercalated discs was markedly reduced, suggesting disease-associated channel redistribution. Additionally, diabetic patients without ventricular remodeling exhibited lower SK3 expression in this region, supporting a role for metabolic comorbidities in early electrical remodeling, including alterations in intercellular coupling [38]. Given the importance of intercalated discs in electrical and mechanical coupling, such changes may have arrhythmogenic implications. These remodeling events may be mediated by alterations in intracellular signaling, cytoskeletal anchoring, or trafficking pathways, mechanisms previously implicated in AF and cardiac hypertrophy [8,23,25,39].

Moreover, SK2 and SK3 can form heteromeric channels in cardiac tissue [4,37,40]. When dual-stained for SK2 and SK3, the striated pattern of SK2 appeared less defined, potentially due to spatial

proximity or interaction between isoforms, impairing the antibody access and reinforcing the hypothesis of heteromeric conformation of SK isoforms. The specific subunit composition of SK channels may influence calcium sensitivity, gating kinetics, and subcellular localization. Collectively, our findings highlight a complex and isoform-specific regulation of SK channels in early ventricular remodeling.

4.4 Functional characterization of SK channels in human ventricular slices

To investigate SK channel functionality, we utilized ultrathin cardiac slices from patient biopsies [26], a model that preserves native tissue architecture and multicellularity [28]. This contrasts with isolated cardiomyocytes, in which enzymatic processes during the isolation may disrupt native channel localization and function.

Here, we assessed the response to 1 µM apamin, a selective channel blocker, in the presence of 100 nM isoprenaline to enhance I_{SK} by increasing intracellular Ca^{2+} and reducing voltage-dependent rectification [25,35]. Apamin significantly prolonged APD_{80} in remodeled myocardium, whereas no effect was observed in non-remodeled slices (Figure 4). These results align with prior work [11] showing increased sensitivity to SK inhibition in failing ventricular myocytes and suggest functional recruitment of SK channels in early remodeling, as in our cohort of patients with valvular disease and in the cohort of patients with aortic stenosis and preserved LVEF of previous studies [11]. However, in other studies using other inhibitors of SK channel activity, no effects on ventricular repolarization have been observed in interventricular septal tissues of patients with valvular pathologies [35], highlighting the potential differences related to disease stage or the pharmacological profile of the inhibitors used.

Our findings further caution against indiscriminate SK channel inhibition in patients with structural ventricular disease. Notably, a recent phase 2 clinical trial of the SK channel inhibitor AP30663 reported high cardioversion rates in AF without significant adverse effects [9]. However, patients with valvular disease or recent bypass surgery, conditions present in our cohort, were excluded, emphasizing the need for careful patient selection in future trials.

Application of the SK channel activator SKA-31 (100 µM) significantly shortened APD_{80} in remodeled, but not in non-remodeled, slices (Figure 5). The effect was more pronounced in patients with reduced LVEF (Figure 6B), suggesting progressive recruitment of SK channels during remodeling. No differences in response were observed with respect to sex, age, or biopsy type. Despite regional variability in APD_{80}, the response to SKA-31 was consistent between remodeled papillary muscles and septal slices. This suggests that remodeled left ventricular transmural biopsies might respond similarly to SKA-31 activation. It has to be taken into account that we used a relatively high concentration of the SK channel activator SKA-31 exceeds its reported EC50 (in the low micromolar range [41,42]), and is higher than the concentrations typically

used in isolated cell or tissue studies [43,44], and may result in off-target effects. Although no significant effects were observed in non-remodeled tissue, suggesting specificity, non-specific effects cannot be ruled-out.

In addition, it should be considered that SKA-31 may also affect mitochondrial SK channels, which are not inhibited by apamin and have been implicated in the regulation of mitochondrial membrane potential, reactive oxygen species production, and intracellular Ca^{2+} handling. Recent evidence indicates that mito-SK channels may contribute to cardioprotection by modulating mitochondrial redox balance and intracellular Ca^{2+} homeostasis rather than directly influencing sarcolemmal electrophysiological properties [45].

Therefore, while some contribution of mitochondrial SK channels to the observed effects cannot be excluded, their role is likely indirect. In contrast, the changes in APD_{80} observed in our study are more consistent with activation of sarcolemmal SK channels, which directly couple intracellular Ca^{2+} dynamics to membrane repolarization. This interpretation is further supported by the absence of SKA-31 effects in non-remodeled myocardium and by the predominant T-tubular localization observed in our immunohistochemical analysis. Importantly, these differential functional responses were not paralleled by consistent mRNA or protein upregulation, suggesting that post-translational mechanisms drive SK channel recruitment during early disease stages. *KNNN2* and *KCNN3* transcript levels remained unchanged in remodeled myocardium, despite clear functional evidence. Our immunolohistological analysis further revealed differential expression patterns of SK2 and SK3 channels between remodeled and non-remodeled tissue. While SK3 protein expression did not show a statistically significant increase and SK2 expression was reduced, these findings, together with the absence of an apamin-sensitive effect in non-remodeled myocardium, despite SK channel expression, indicate that SK channel activity is not only determined by gene or protein expression levels but rather post-translational regulation, intracellular signaling pathways and intracellular Ca^{2+} handling.

4.5 Mechanisms of SK channel recruitment in ventricular remodeling

To elucidate the molecular mechanisms underlying SK channel activation in remodeled myocardium, we examined the effects of SKA-31 after pharmacological inhibition of proteins known to modulate SK channel activation.

Pre-treatment with nifedipine, an LTCC blocker, completely abrogated the response to SKA-31, confirming that Ca^{2+} influx through LTCCs is necessary for SK channel activation (Figure 7A). This is consistent with evidence of SK channel colocalization and functional coupling to LTCCs via α-actinin2 [19,21]. Although we did not assess RyR contributions, prior studies in isolated rat ventricular cardiomyocytes suggest that Ca^{2+} contribution from RyRs supports SK channel

activation [20]. This suggests that SK channels might depend on multiple sources of Ca^{2+} for activation, particularly under pathological conditions involving altered Ca^{2+} handling.

CaMKII is a key Ca^{2+}-sensitive protein known to modulate multiple ion channels and Ca^{2+} handling processes, and has been reported to phosphorylate SK channels and enhance their Ca^{2+} sensitivity [16]. In our study, its inhibition with KN-93 or with a more selective inhibitor like AIP [46] similarly prevented APD_{80} shortening in response to SKA-31 (Figures 7B and 7C respectively), supporting the hypothesis that CaMKII might be involved in the modulation of SK channels. However, given the broad role of CaMKII, this effect may not be specific to direct SK channel modulation, but could also be mediated through alterations in intracellular Ca^{2+} handling or other downstream targets. These findings align with studies demonstrating increased CaMKII activity in hypertrophied and failing hearts, where it contributes to Ca^{2+} dysregulation and arrhythmogenesis [23,24,47].

Conversely, inhibition of PKA with H-89 had no effect on SKA-31-induced responses, suggesting that PKA does not acutely modulate SK channel function under our conditions (Figure 7D and 7E). While PKA has been shown to enhance I_{SK} by reducing Ca^{2+}/voltage-dependent inhibition [25] and modulating SK channel trafficking and membrane expression [48,49], a role for PKA in long-term channel trafficking and transcriptional regulation cannot be excluded.

4.6 Study limitations

First, gene expression and functional assessments were conducted in anatomically non-equivalent regions. Consequently, the results should be interpreted with caution, particularly given prior reports of heterogeneous SK channel upregulation in disease [11]. This limitation primarily stems from differences in surgical accessibility: during coronary artery bypass grafting, only transmural biopsies can be obtained, whereas valve replacement procedures allow access to papillary muscles and septal biopsies. Nevertheless, in the immunohistochemical analysis, comparable anatomical regions were examined between remodeled and non-remodeled tissues. Interestingly, SK2 expression levels were higher in non-remodeled myocardium, whereas SK3 expression was more similar between non-remodeled epicardium and remodeled papillary muscles / interventricular septum than between non-remodeled and remodeled epicardium. These findings make the observed functional differences particularly noteworthy and underscore the importance of functional assessment to elucidate potential regulatory mechanisms.

A further limitation concerns the use of electromechanical uncouplers (BDM and blebbistatin), during optical mapping experiments to prevent tissue movement. These agents are known to modulate several ionic currents, including potassium currents [50,51], which may have indirectly influenced SK channel function.

Additionally, patient-related heterogeneity represents an inherent limitation. The ventricular remodeling group encompasses individuals with varying types and degrees of valvular heart disease, while the non-remodeled group cannot be considered entirely healthy controls. Although only patients with preserved LVEF and no hypertrophy were included, all underwent coronary artery bypass grafting, and subclinical remote remodeling secondary to ischemia cannot be excluded. Other factors, including age, sex and comorbidities, may also affect channel expression and function. While efforts were made to assess the influence of these variables, the sample size, though relatively large compared to other studies using human ventricular tissue, was insufficient to evaluate all potential sources of variability comprehensively.

4.7 Conclusion

Our findings indicate that upregulation of SK channel in remodeled ventricular tissue is not driven by transcriptional changes but rather by regional remodeling and complex post-translational mechanisms. Although mRNA levels of *KCNN2* or *KCNN3* remain unchanged, SK2 protein expression is slightly decreased and SK3 displays heterogeneous distribution, marked by increased expression in the remodeled epicardium and decreased localization at intercalated discs across all remodeled regions. Functional analyses show that SK channels are inactive in non-remodeled ventricles but become functionally active in early stages of remodeling. This activation is dependent on calcium influx via LTCCs and is abolished by CaMKII inhibition, while PKA inhibition has no effect, suggesting a minimal role for PKA in acute SK channel regulation. Collectively, these results support the concept that SK channels are quiescent under physiological conditions but are functionally recruited during pathological remodeling, likely due to altered intracellular calcium signaling.

Funding

The article was funded by Agencia Estatal de Investigación—Ministerio de Ciencia e Innovación (Spain) through projects PID2022-140556OB-I00 and TED2021-130459B-I00 and by Gobierno de Aragón through research group T39_23R. Computations were performed using ICTS NANBIOSIS (HPC Unit at University of Zaragoza). A.P.M. was supported by a predoctoral fellowship from the Departamento de Ciencia, Universidad y Sociedad del Conocimiento from the Gobierno de Aragón 2020-2024 (CUS/581/2020).

CRediT author statement

Alba Pérez-Martínez: Conceptualization, Methodology, Validation, Formal analysis, Investigation, Data Curation, Writing-Original Draft, Writing- Review & Editing, Visualization. **Cristina López-Andrés**: Formal analysis, Investigation. **Laura García-Mendívil**: Formal analysis, Investigation, Writing- Review & Editing. **Marta López-Yus**: Formal analysis,

Investigation. **Diana Batín**: Resources. **Jose M. Vallejo-Gil**: Resources. **Javier Fañanás-Mastral**: Resources. **Manuel Vázquez-Sancho**: Resources. **Marta Matamala-Adell**: Resources. **Juan F. Sorribas-Berjon**: Resources. **Javier A. Bellido-Morales**: Resources. **Carlos Ballester-Cuenca**: Resources. **Jose M. Arbonés Mainar**: Resources, Writing- Review & Editing. **Esther Pueyo**: Conceptualization, Validation, Writing-Original Draft, Writing- Review & Editing, Supervision, Funding acquisition. **Aída Oliván-Viguera**: Conceptualization, Methodology, Investigation, Validation, Writing-Original Draft, Writing- Review & Editing, Supervision, Project administration.

All authors have read and approved the final version of the manuscript.

Acknowledgements

The authors wish to thank all patients and the anesthesiologists, perfusionists and nurses of the Cardiovascular Surgery Department at Miguel Servet University Hospital. Authors wish to also thank the Anatomic Pathology Core Unit and the Imaging and Microscopy Core Unit of Aragón Health Sciences Institute (IACS) for their contribution to histological processing and imaging. *KCNN2* primers were kindly provided by Natalia Hernandez Bellido and Laura Ordovás.

Data availability

Data will be shared on reasonable request to the corresponding author.

Disclosures

None declared.

Declaration of generative AI and AI-assisted technologies in the writing process

The authors did not use generative AI or AI-assisted technologies in the development of this manuscript.

Journal Pre-proof

References

1. Xu Y, Tuteja D, Zhang Z, Xu D, Zhang Y, Rodriguez J, et al. Molecular Identification and Functional Roles of a Ca2+-activated K+ Channel in Human and Mouse Hearts *. *J Biol Chem* 2003;**278**:49085–49094.

2. Lee W-S, Ngo-Anh TJ, Bruening-Wright A, Maylie J, Adelman JP. Small conductance Ca2+-activated K+ channels and calmodulin: cell surface expression and gating. *J Biol Chem* 2003;**278**:25940–25946.

3. Yu C-C, Corr C, Shen C, Shelton R, Yadava M, Rhea IB, et al. Small conductance calcium-activated potassium current is important in transmural repolarization of failing human ventricles. *Circ Arrhythm Electrophysiol* 2015;**8**:667–676.

4. Butler AS, Hancox JC, Marrion NV. Preferential formation of human heteromeric SK2:SK3 channels limits homomeric SK channel assembly and function. *J Biol Chem* 2023;**299**.

5. Nagy N, Szuts V, Horváth Z, Seprényi G, Farkas AS, Acsai K, et al. Does small-conductance calcium-activated potassium channel contribute to cardiac repolarization? *J Mol Cell Cardiol* 2009;**47**:656–663.

6. Christophersen P, Wulff H. Pharmacological gating modulation of small- and intermediate-conductance Ca2+-activated K+ channels (KCa2.x and KCa3.1). *Channels* 2015;**9**:336–343.

7. Diness JG, Skibsbye L, Jespersen T, Bartels ED, Sørensen US, Hansen RS, et al. Effects on Atrial Fibrillation in Aged Hypertensive Rats by Ca2+-Activated K+ Channel Inhibition. *Hypertension* 2011;**57**:1129–1135.

8. Heijman J, Zhou X, Morotti S, Molina CE, Abu-Taha IH, Tekook M, et al. Enhanced Ca2+-Dependent SK-Channel Gating and Membrane Trafficking in Human Atrial Fibrillation. *Circ Res* 2023;**132**:e116–e133.

9. Holst AG, Tomcsányi J, Vestbjerg B, Grunnet M, Sørensen US, Diness JG, et al. Inhibition of the KCa2 potassium channel in atrial fibrillation: a randomized phase 2 trial. *Nat Med* 2024;**30**:106–111.

10. Bonilla IM, Iii VPL, Vargas-Pinto P, Wright P, Belevych A, Lou Q, et al. Calcium-Activated Potassium Current Modulates Ventricular Repolarization in Chronic Heart Failure. *PLOS ONE* 2014;**9**:e108824.

11. Chang P-C, Turker I, Lopshire JC, Masroor S, Nguyen B-L, Tao W, et al. Heterogeneous upregulation of apamin-sensitive potassium currents in failing human ventricles. *J Am Heart Assoc* 2013;**2**:e004713.

12. Chang P-C, Chen P-S. SK channels and ventricular arrhythmias in heart failure. *Trends Cardiovasc Med* 2015;**25**:508–514.

13. Gu M, Zhu Y, Yin X, Zhang D-M. Small-conductance Ca2+-activated K+ channels: insights into their roles in cardiovascular disease. *Exp Mol Med* 2018;**50**:1–7.

14. Lee YS, Chang P-C, Hsueh C-H, Maruyama M, Park HW, Rhee K-S, et al. Apamin-Sensitive Calcium-Activated Potassium Currents in Rabbit Ventricles with Chronic Myocardial Infarction. *J Cardiovasc Electrophysiol* 2013;**24**:1144–1153.

15. Mahida S. Expanding role of SK channels in cardiac electrophysiology. *Heart Rhythm* 2014;**11**:1233–1238.

16. Ni Y, Wang T, Zhuo X, Song B, Zhang J, Wei F, et al. Bisoprolol reversed small conductance calcium-activated potassium channel (SK) remodeling in a volume-overload rat model. *Mol Cell Biochem* 2013;**384**:95–103.

17. Bronk P, Kim TY, Polina I, Hamilton S, Terentyeva R, Roder K, et al. Impact of ISK Voltage and Ca2+/Mg2+-Dependent Rectification on Cardiac Repolarization. *Biophys J* 2020;**119**:690–704.

18. Rafizadeh S, Zhang Z, Woltz RL, Kim HJ, Myers RE, Lu L, et al. Functional interaction with filamin A and intracellular Ca^{2+} enhance the surface membrane expression of a small-conductance Ca^{2+}-activated K^{+} (SK2) channel. *Proc Natl Acad Sci USA* 2014;**111**:9989–9994.

19. Zhang X-D, Coulibaly Z, Chen WC, Ledford HA, Jeong Han Lee, Lee JH, et al. Coupling of SK channels, L-type Ca2+ channels, and ryanodine receptors in cardiomyocytes. *Sci Rep* 2018;**8**:4670–4670.

20. Terentyev D, Rochira JA, Terentyeva R, Roder K, Koren G, Li W. Sarcoplasmic reticulum Ca^{2+} release is both necessary and sufficient for SK channel activation in ventricular myocytes. *Am J Physiol Heart Circ Physiol* 2014;**306**:H738-746.

21. Lu L, Zhang Q, Timofeyev V, Zhang Z, Young JN, Shin H-S, et al. Molecular coupling of a Ca2+-activated K+ channel to L-type Ca2+ channels via alpha-actinin2. *Circ Res* 2007;**100**:112–120.

22. Fan X, Yu Y, Lan H, Ou X, Yang L, Li T, et al. Ca2+/Calmodulin-Dependent Protein Kinase II (CaMKII) Increases Small-Conductance Ca2+-Activated K+ Current in Patients with Chronic Atrial Fibrillation. *Med Sci Monit* 2018;**24**:3011–3023.

23. Mizukami K, Yokoshiki H, Mitsuyama H, Watanabe M, Tenma T, Takada S, et al. Small-conductance Ca2+-activated K+ current is upregulated via the phosphorylation of CaMKII in cardiac hypertrophy from spontaneously hypertensive rats. *AJP-Heart and Circ Physiol* 2015;**309**:H1066–H1074.

24. Tenma T, Mitsuyama H, Watanabe M, Kakutani N, Otsuka Y, Mizukami K, et al. Small-conductance Ca2+-activated K+ channel activation deteriorates hypoxic ventricular arrhythmias via CaMKII in cardiac hypertrophy. *Am J Physiol Heart Circ Physiol* 2018;**315**:H262–H272.

25. Hamilton S, Polina I, Terentyeva R, Bronk P, Kim TY, Roder K, et al. PKA phosphorylation underlies functional recruitment of sarcolemmal SK2 channels in ventricular myocytes from hypertrophic hearts. *J Physiol* 2020;**598**:2847–2873.

26. Oliván-Viguera A, Pérez-Zabalza M, García-Mendívil L, Mountris KA, Orós-Rodrigo S, Ramos-Marquès E, et al. Minimally invasive system to reliably characterize ventricular electrophysiology from living donors. *Sci Rep* 2020;**10**:19941.

27. Perez-Zabalza M, Diez E, Rhyins J, Mountris K, Vallejo-Gil J, Fresneda-Roldán P, et al. Improved Methods for Processing Optical Mapping Signals From Human Left Ventricular Tissues at Baseline and Following Adrenergic Stimulation. *CinC* 2020;**47**:1–4.

Journal Pre-proof

28. Watson SA, Scigliano M, Bardi I, Ascione R, Terracciano CM, Perbellini F. Preparation of viable adult ventricular myocardial slices from large and small mammals. *Nat Protoc* 2017;**12**:2623–2639.

29. Nattel S, Maguy A, Le Bouter S, Yeh Y-H. Arrhythmogenic ion-channel remodeling in the heart: heart failure, myocardial infarction, and atrial fibrillation. *Physiol Rev* 2007;**87**:425–456.

30. Soltysinska E, Olesen S-P, Christ T, Wettwer E, Varró A, Grunnet M, et al. Transmural expression of ion channels and transporters in human nondiseased and end-stage failing hearts. *Pflugers Arch - Eur J Physiol* 2009;**459**:11–23.

31. Chang P-C, Hsieh Y-C, Hsueh C-H, Weiss JN, Lin S-F, Chen P-S. Apamin induces early afterdepolarizations and torsades de pointes ventricular arrhythmia from failing rabbit ventricles exhibiting secondary rises in intracellular calcium. *Heart Rhythm* 2013;**10**:1516–1524.

32. Darkow E, Nguyen TT, Stolina M, Kari FA, Schmidt C, Wiedmann F, et al. Small Conductance Ca2 +-Activated K+ (SK) Channel mRNA Expression in Human Atrial and Ventricular Tissue: Comparison Between Donor, Atrial Fibrillation and Heart Failure Tissue. *Front Physiol* 2021;**12**:342.

33. Félétou M. Calcium-activated potassium channels and endothelial dysfunction: therapeutic options? *Br J Pharmacol* 2009;**156**:545–562.

34. Grgic I, Kaistha BP, Hoyer J, Köhler R. Endothelial Ca2+-activated K+ channels in normal and impaired EDHF–dilator responses – relevance to cardiovascular pathologies and drug discovery. *Br J Pharmacol* 2009;**157**:509–526.

35. Skibsbye L, Poulet C, Diness JG, Bentzen BH, Yuan L, Kappert U, et al. Small-conductance calcium-activated potassium (SK) channels contribute to action potential repolarization in human atria. *Cardiovasc Res* 2014;**103**:156–167.

36. Tuteja D, Rafizadeh S, Timofeyev V, Wang S, Zhang Z, Li N, et al. Cardiac small conductance Ca2+-activated K+ channel subunits form heteromultimers via the coiled-coil domains in the C termini of the channels. *Circ Res* 2010;**107**:851–859.

37. Hancock JM, Weatherall KL, Choisy SC, James AF, Hancox JC, Marrion NV. Selective activation of heteromeric SK channels contributes to action potential repolarization in mouse atrial myocytes. *Heart Rhythm* 2015;**12**:1003–1015.

38. Tse G, Lai ETH, Tse V, Yeo JM. Molecular and Electrophysiological Mechanisms Underlying Cardiac Arrhythmogenesis in Diabetes Mellitus. *J Diabetes Res* 2016;**2016**:2848759.

39. Chen M, Fei Y, Chen T-Z, Li Y-G, Chen P-S. The regulation of the small-conductance calcium-activated potassium current and the mechanisms of sex dimorphism in J wave syndrome. *Pflugers Arch* 2021;**473**:491–506.

40. Qi M-M, Qian L, Wang R-X. Modulation of SK Channels: Insight Into Therapeutics of Atrial Fibrillation. *Heart Lung Circ* 2021;**30**:1130–1139.

41. Sankaranarayanan A, Raman G, Busch C, Schultz T, Zimin PI, Hoyer J, et al. Naphtho[1,2-d]thiazol-2-ylamine (SKA-31), a new activator of KCa2 and KCa3.1 potassium channels,

potentiates the endothelium-derived hyperpolarizing factor response and lowers blood pressure. *Mol Pharmacol* 2009;**75**:281–295.

42. Sforna L, Megaro A, Pessia M, Franciolini F, Catacuzzeno L. Structure, Gating and Basic Functions of the Ca2+-activated K Channel of Intermediate Conductance. *Curr Neuropharmacol* 2018;**16**:608–617.

43. Kloza M, Baranowska-Kuczko M, Toczek M, Kusaczuk M, Sadowska O, Kasacka I, et al. Modulation of Cardiovascular Function in Primary Hypertension in Rat by SKA-31, an Activator of KCa2.x and KCa3.1 Channels. *International Journal of Molecular Sciences* 2019;**20**:4118.

44. Mishra RC, Wulff H, Cole WC, Braun AP. A pharmacologic activator of endothelial KCa channels enhances coronary flow in the hearts of type 2 diabetic rats. *J Mol Cell Cardiol* 2014;**72**:364–373.

45. Terentyev D, Glukhov AV, Bogdanov V, Averin AS, Veress R, Choi B-R, et al. Small-Conductance Ca2+-Activated K+ Channels in Cardiac Excitation–Contraction Coupling: Bridging Mitochondria, Sarcolemma, and Antiarrhythmic Therapy. *J Physiol* 2025:10.1113/JP289566.

46. Daniels LJ, Wallace RS, Nicholson OM, Wilson GA, McDonald FJ, Jones PP, et al. Inhibition of calcium/calmodulin-dependent kinase II restores contraction and relaxation in isolated cardiac muscle from type 2 diabetic rats. *Cardiovasc Diabetol* 2018;**17**:89.

47. Anderson ME, Brown JH, Bers DM. CaMKII in myocardial hypertrophy and heart failure. *J Mol Cell Cardiol* 2011;**51**:468–473.

48. Nam Y-W, Kong D, Wang D, Orfali R, Sherpa RT, Totonchy J, et al. Differential modulation of SK channel subtypes by phosphorylation. *Cell Calcium* 2021;**94**:102346.

49. Ren Y, Barnwell LF, Alexander JC, Lubin FD, Adelman JP, Pfaffinger PJ, et al. Regulation of surface localization of the small conductance Ca2+-activated potassium channel, Sk2, through direct phosphorylation by cAMP-dependent protein kinase. *J Biol Chem* 2006;**281**:11769–11779.

50. Brack KE, Narang R, Winter J, Ng GA. The mechanical uncoupler blebbistatin is associated with significant electrophysiological effects in the isolated rabbit heart. *Exp Physiol* 2013;**98**:1009–1027.

51. Watanabe Y, Iwamoto T, Matsuoka I, Ohkubo S, Ono T, Watano T, et al. Inhibitory effect of 2,3-butanedione monoxime (BDM) on Na+/Ca2+ exchange current in guinea-pig cardiac ventricular myocytes. *Br J Pharmacol* 2001;**132**:1317–1325.

Journal Pre-proof

Figures

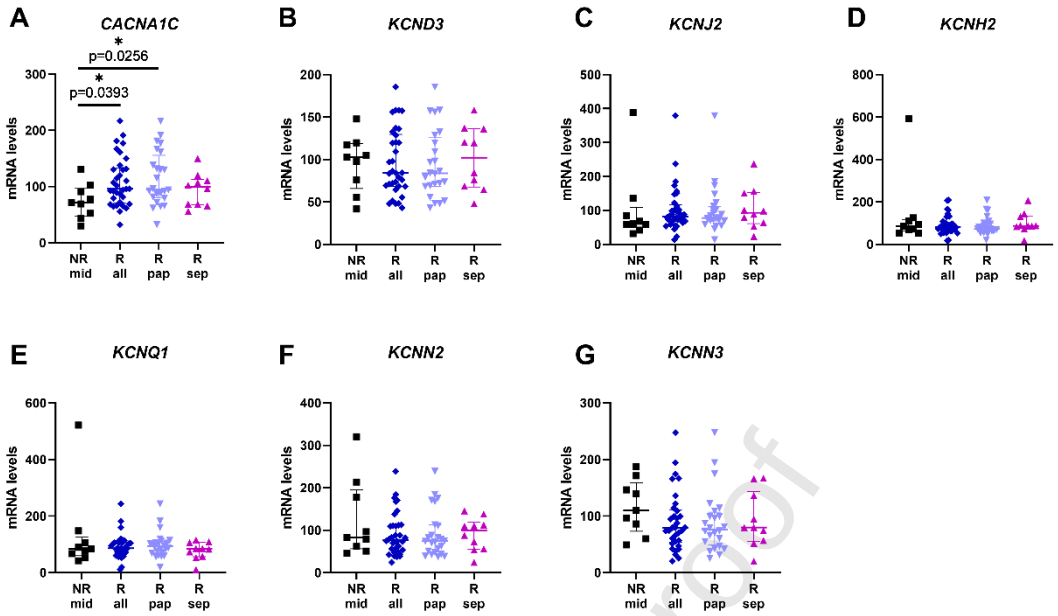


Figure 1: mRNA expression of **A)** *CACNA1*, **B)** *KCND3*, **C)** *KCNJ2*, **D)** *KCNH2*, **E)** *KCNQ1*, **F)** *KCNN2*, and **G)** *KCNN3* of NR mid: non-remodeled mid-myocardium (N = 9), R pap: remodeled papillary muscles (N = 24), R sep: remodeled septum (N = 10), R all: remodeled papillary muscles and septum samples. Relative gene expression was normalized to *GAPDH* (= 100%). P values are given for Mann-Whitney test comparing mRNA expression levels between different groups.

Journal Pre-proof

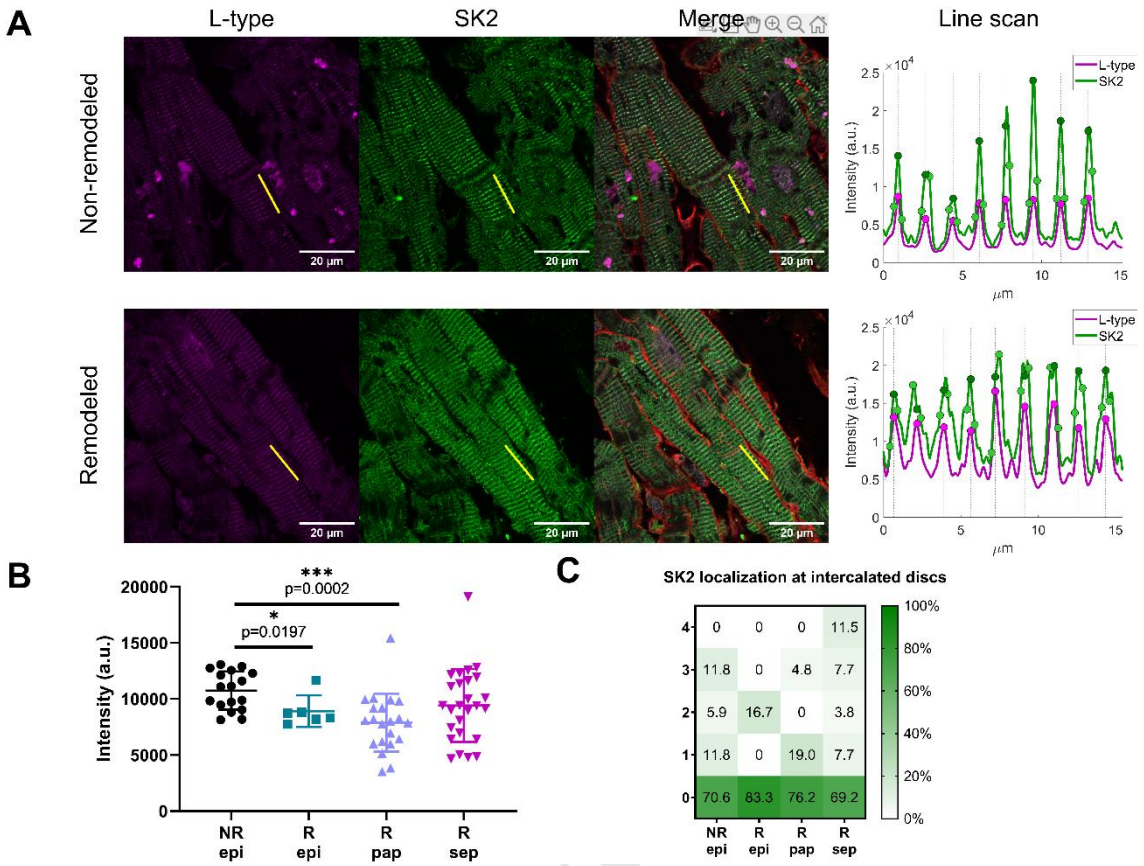


Figure 2: SK2 protein expression and location in relation to L-type Ca^{+2} channels. A) confocal image at 100X magnification of representative non-remodeled myocardium (above) and remodeled myocardium (below) stained with L-Type Ca^{2+} channels (magenta), SK2 (green), and Wheat Germ Agglutinin (WGA, red) with plots of fluorescence profiles (line scans) corresponding with the yellow lines in each image. **B)** fluorescence intensity levels at the detected peaks (striations). P values are given for Mann-Whitney test comparing expression levels between different groups. **C)** scores for SK2 location at intercalated discs of the different groups of patients. NR epi: non-remodeled epicardium (N = 17), R epi: remodeled epicardium (N = 6), R pap: remodeled papillary muscles (N = 21), R sep: remodeled septum (N = 26).

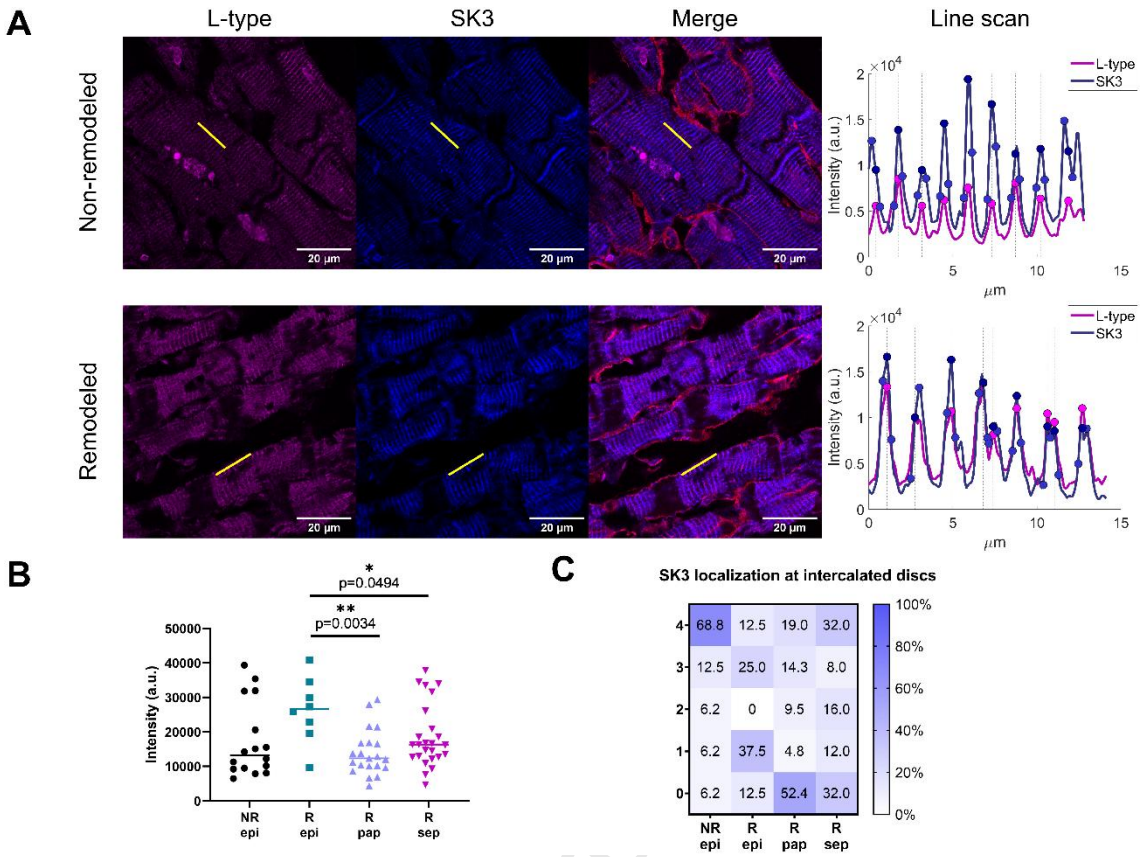


Figure 3: SK3 protein expression and location in relation to L-type Ca^{+2} channels. A) confocal image at 100X magnification of representative non-remodeled myocardium (above) and remodeled myocardium (below) stained with L-Type Ca^{2+} channels (magenta), SK3 (blue), and Wheat Germ Agglutinin (WGA, red) with plots of fluorescence profiles (line scans) corresponding with the yellow lines in each image. **B)** fluorescence intensity levels at the detected peaks (striations). P values are given for Mann-Whitney test comparing expression levels between different groups. **C)** scores for SK3 location at intercalated discs of the different groups of patients. NR epi: non-remodeled epicardium (N = 16), R epi: remodeled epicardium (N = 8), R pap: remodeled papillary muscles (N = 21), R sep: remodeled septum (N = 25).

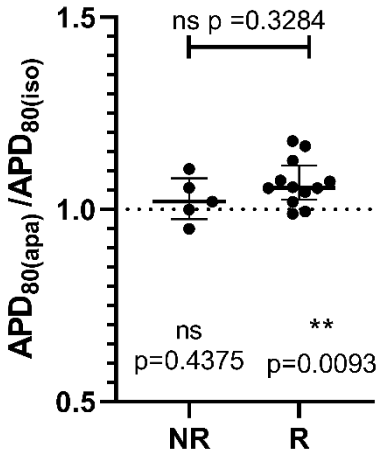


Figure 4: Response to 1 µM apamin after incubation with 100 nM isoprenaline at 1 Hz pacing frequency in human biopsies of non-remodeled (n/N = 16/5) and remodeled (n/N = 38/12) myocardium. NR: non-remodeled, R: remodeled. The p values in the bottom of the graphic correspond to the Wilcoxon signed-rank test comparing the effects of apamin on APD_{80} with respect to the isoprenaline state separately for non-remodeled and remodeled ventricular tissues. The p value in the top corresponds to the Mann-Whitney comparing remodeled and non-remodeled tissues.

Journal Pre-proof

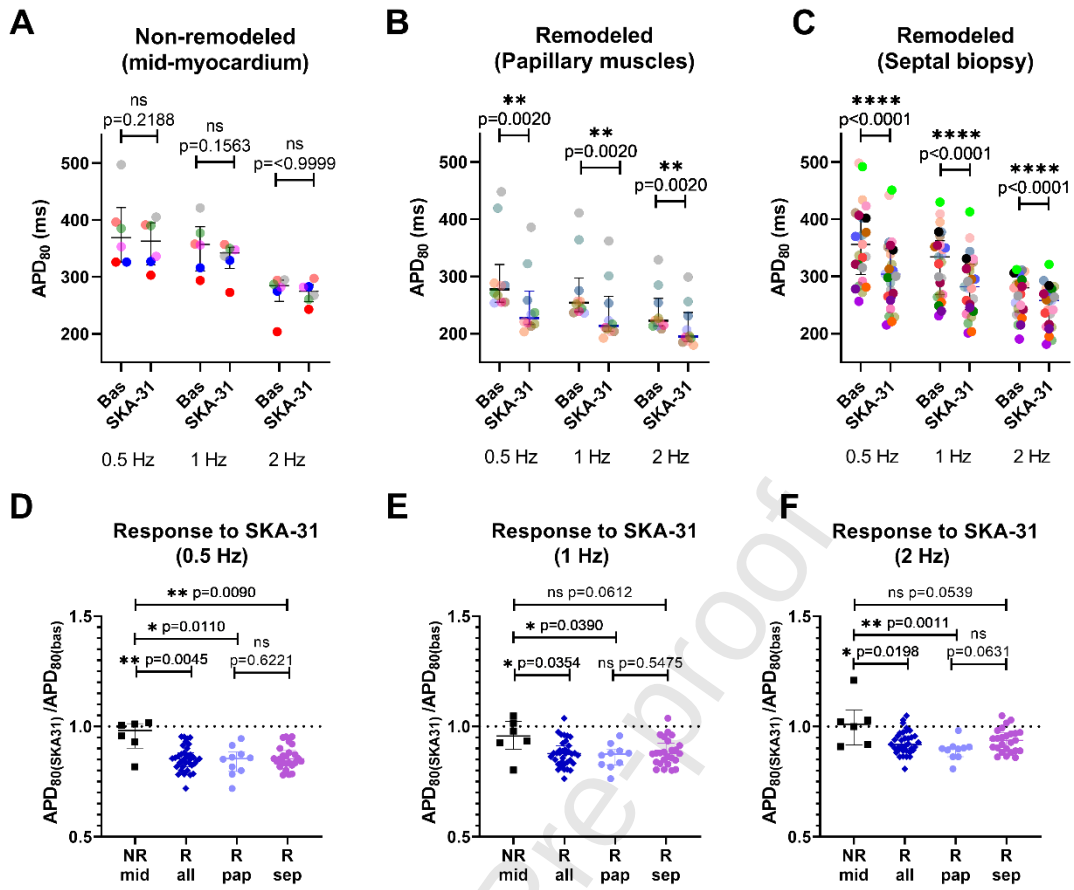


Figure 5: Response to 100 µM SKA-31 at different pacing frequencies in human biopsies of **A)** non-remodeled myocardium (n/N = 20/6), **B)** papillary muscles (n/N = 37/10), and **C)** interventricular septum (n/N = 83/25) of patients with ventricular remodeling. Comparison of the response to 100 µM SKA-31 at **D)** 0.5, **E)** 1 and **F)** 2 Hz pacing frequency in the different groups of patients: NR mid: non-remodeled mid-myocardium (n/N = 20/6), R pap: remodeled papillary muscles (n/N = 37/10), R sep: remodeled septum (n/N = 83/25). P values are given for Wilcoxon signed-rank test for paired samples in A to C, and for Mann-Whitney test for D to F.

Journal Pre-proof

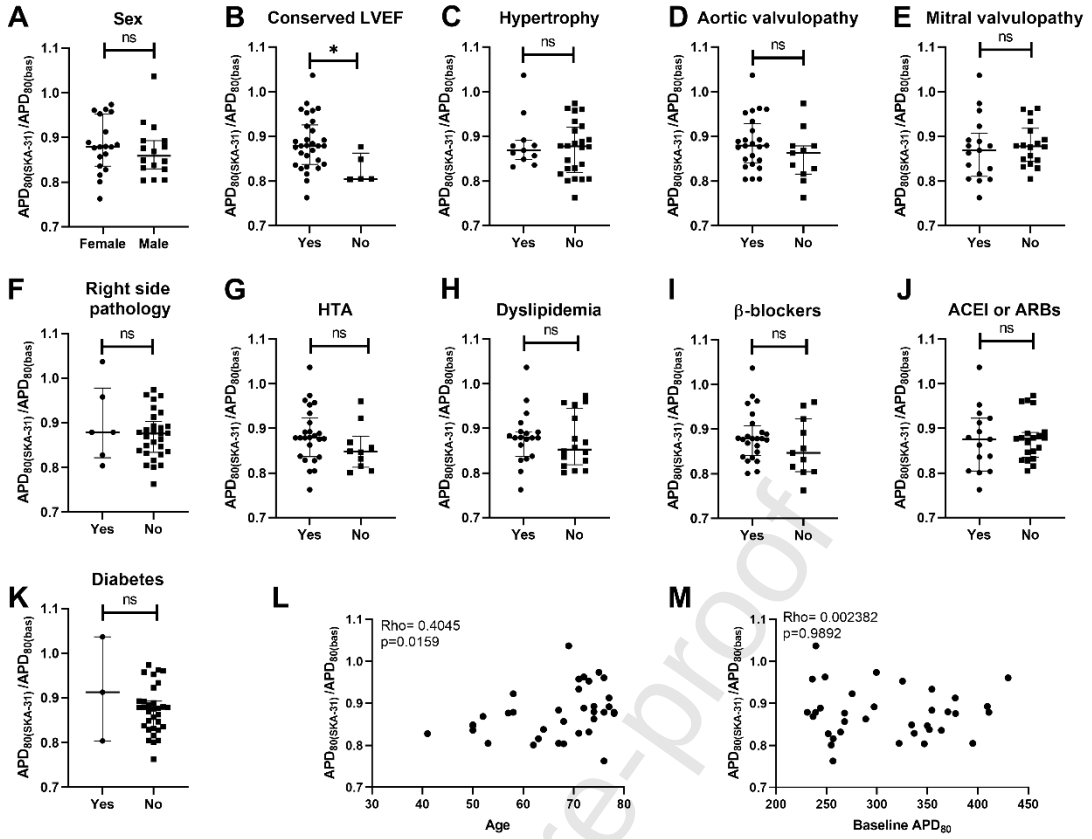


Figure 6. Response to 100 µM SKA-31 in remodeled myocardium (n/N = 120/35) according to the following factors: **A)** sex (p = 0.2267), **B)** preserved LVEF (*p = 0.0103), **C)** hypertrophy (p = 0.7728), **D)** aortic valvulopathy (p = 0.5691), **E)** mitral valvulopathy (p = 0.7138), **F)** right side valvular disfunction (p = 0.4470), **G)** arterial hypertension (HBP, p = 0.2823), **H)** dyslipidemia (p = 0.8766), **I)** treatment with β-blockers (p = 0.2009), **J)** treatment with angiotensin converting enzyme or angiotensin receptor blockers (ACEI or ARBs, p = 0.3257) and **K)** diabetes (p = 0.5638). Correlation of the response to SKA-31 versus **L)** age, and **M)** baseline APD_{80}. Dots indicate individual patients. Correlation values and p values (Spearman) are shown. P values from A to K are for Mann-Whitney tests.

Journal Pre-proof

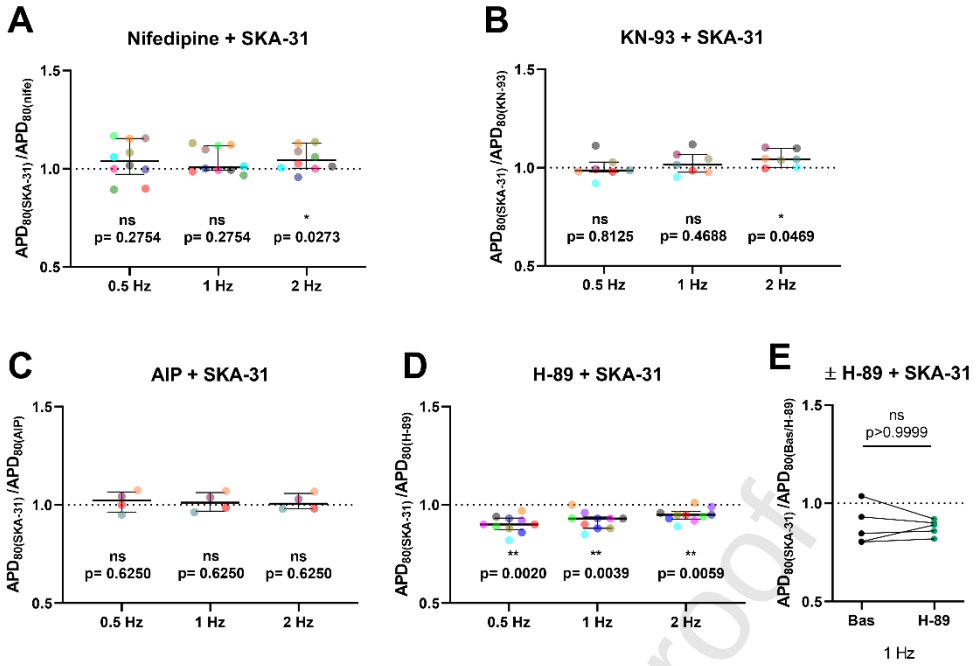
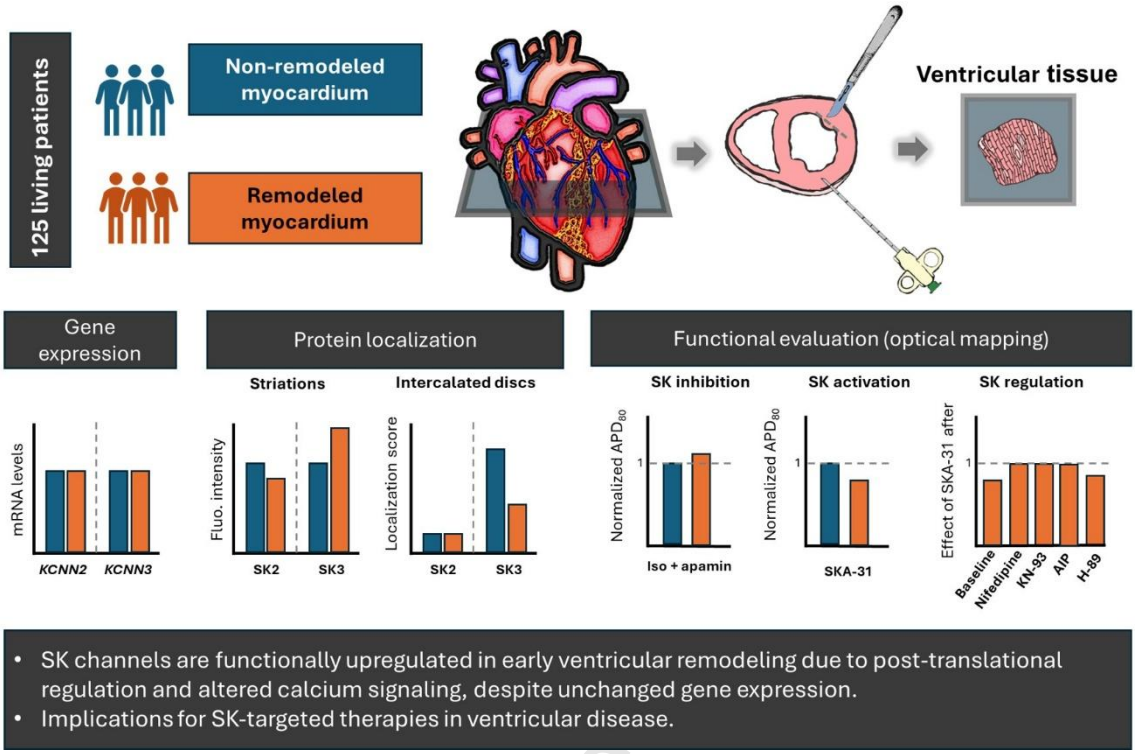


Figure 7. Functional regulation of SK channels. Response of remodeled myocardium (papillary muscles and septal biopsies) to 100 µM SKA-31 at 0.5, 1, and 2 Hz pacing frequencies after incubation with **A)** 10 µM nifedipine (nife, n/N = 30/10), **B)** 2 µM KN-93 (n/N = 23/7), **C)** 10 µM AIP (n/N = 12/4), **D)** 2 µM H-89 (n/N = 27/10). **E)** response to 100 µM SKA-31 from the same patients after baseline conditions or after incubation with 2 µM H-89 (n/N = 11-13/5). P values are given for Wilcoxon signed-rank test for paired samples comparing APD_{80} before and after the addition of SKA-31, except for D which is Mann-Whitney comparing the response to SKA-31 between the two groups.

Journal Pre-proof

Graphical abstract



- SK channels are functionally upregulated in early ventricular remodeling due to post-translational regulation and altered calcium signaling, despite unchanged gene expression.
- Implications for SK-targeted therapies in ventricular disease.

Journal Pre-proof

Journal Pre-proof

Highlights

- SK2 and SK3 channels are expressed in human ventricular myocardium
- Human ventricular remodeling induces functional upregulation of SK channels
- Ventricular SK activation occurs despite preserved *KCNN2/3* expression levels
- SK channel modulation depends on Ca^{2+} handling and CAMKII signaling
- Atria-selective SK targeting may affect remodeled ventricles in AF patients

Journal Pre-proof